

Lattice QCD calculation of hadronic light-by-light scattering

Jeremy Green^a, Oleksii Gryniuk^{a,c}, Georg von Hippel^a, Harvey B. Meyer^{a,b}, Vladimir Pascalutsa^a

^a*PRISMA Cluster of Excellence & Institut für Kernphysik,
Johannes Gutenberg-Universität Mainz, D-55099 Mainz, Germany*

^b*Helmholtz Institut Mainz, D-55099 Mainz, Germany*

^c*Taras Shevchenko Kyiv National University, Volodymyrska 60, UA-01033 Kyiv, Ukraine**

(Dated: July 7, 2015)

We perform a lattice QCD calculation of the hadronic light-by-light scattering amplitude in a broad kinematical range. At forward kinematics, the results are compared to a phenomenological analysis based on dispersive sum rules for light-by-light scattering. The size of the pion pole contribution is investigated for momenta of typical hadronic size. The presented numerical methods can be used to compute the hadronic light-by-light contribution to the anomalous magnetic moment of the muon. Our calculations are carried out in two-flavor QCD with the pion mass in the range of 270 to 450 MeV, and contain so far only the diagrams with fully connected quark lines.

I. INTRODUCTION

Light-by-light scattering, the elastic scattering of two photons, is a striking prediction of Quantum Electrodynamics (QED). The light-by-light (LbL) interaction appears prominently in corrections to the anomalous magnetic moment ($g - 2$) of the electron and muon. The muon ($g - 2$) exhibits a 3σ discrepancy between experiment and the Standard Model calculations [1]. While the current theory and experimental errors are comparable in size, a new $(g - 2)_\mu$ experiment [2] aiming to reduce the experimental error by a factor of four is in preparation at Fermilab.

The theory error on $(g - 2)_\mu$ is dominated by hadronic contributions, namely the hadronic vacuum polarization (HVP) and hadronic light-by-light (HLbL) scattering. Using unitarity and causality, the HVP contribution is expressed in terms of the total $e^+e^- \rightarrow$ hadrons cross section, and hence its precision can systematically be improved by collider experiments alone. By contrast, the HLbL contribution cannot be expressed entirely in terms of cross sections for $\gamma\gamma$ -fusion into hadrons; see [3–5] for dispersive approaches to the problem. A direct ab initio calculation within Quantum Chromodynamics (QCD) is very challenging due to its non-perturbative nature. In this work we address the problem using lattice QCD.

A first lattice QCD+QED calculation of the HLbL contribution to $(g - 2)_\mu$ has recently been performed by Blum et al. [6]. We envisage a different method where the four-point function for LbL scattering is computed in lattice QCD and integrated over to yield the HLbL contribution. In this Letter we present the four-point function calculation and check it against the available phenomenology. Exploiting unitarity and causality, the forward HLbL amplitude can be expressed as a dispersive integral over the $\gamma^*\gamma^* \rightarrow$ hadrons cross section [7, 8]. A parametrization of the latter allows us to confront the lattice calculation

with phenomenology in a fairly straightforward manner. As the neutral pion (π^0) pole dominates the HLbL contribution to $(g - 2)_\mu$ in phenomenological calculations [1], we study its relative size both at forward and off-forward kinematics.

II. THEORY BACKGROUND

The Lehmann-Symanzik-Zimmermann reduction formula for the HLbL scattering amplitude implies [9]

$$\begin{aligned} \mathcal{M}_{\mu_1\mu_4\mu_2\mu_3}(p_1, p_4 \rightarrow p_2, p_3) \\ = e^4 (-i\Pi_{\mu_1\mu_2\mu_3\mu_4}(-p_4; -p_1, p_2)), \end{aligned} \quad (1)$$

where $p_3 = p_1 + p_4 - p_2$ and

$$\Pi_{\mu_1\mu_2\mu_3\mu_4}(p_4; p_1, p_2) \equiv \int d^4x_1 d^4x_2 d^4x_4 \quad (2)$$

$$e^{+i\sum_a p_a \cdot x_a} \langle 0 | T \{ j_{\mu_1}(x_1) j_{\mu_2}(x_2) j_{\mu_3}(0) j_{\mu_4}(x_4) \} | 0 \rangle$$

is the Minkowski-space time-ordered correlator of the conserved vector current $j_\mu = \frac{2}{3}\bar{u}\gamma_\mu u - \frac{1}{3}\bar{d}\gamma_\mu d + \dots$. The index a takes the values 1, 2 and 4. The components of the current J_μ used in the Euclidean theory [10] are related to their Minkowskian counterparts by $J_0 = j_0$, $J_k = i j_k$. The analytic continuation then yields the following relation to the Euclidean correlation function,

$$-i\Pi_{\mu_1\mu_2\mu_3\mu_4}((-iP_4^0, \vec{P}_4); (-iP_1^0, \vec{P}_1), (-iP_2^0, \vec{P}_2)) \quad (3)$$

$$= i^{n_0} \Pi_{\mu_1\mu_2\mu_3\mu_4}^E(P_4; P_1, P_2),$$

$$\Pi_{\mu_1\mu_2\mu_3\mu_4}^E(P_4; P_1, P_2) \equiv \int d^4X_1 d^4X_2 d^4X_4 \quad (4)$$

$$e^{-i\sum_a P_a \cdot X_a} \left\langle J_{\mu_1}(X_1) J_{\mu_2}(X_2) J_{\mu_3}(0) J_{\mu_4}(X_4) \right\rangle_E,$$

where n_0 is the number of temporal indices carried by the vector currents in the correlator.

The forward scattering case is obtained in Eq. (1) by setting $p_2 = p_1$. Renaming the momenta to match the conventional notation, we have

$$\mathcal{M}_{\mu_1\mu_2\mu_3\mu_4}^{\text{forw}}(q_1, q_2) \equiv \mathcal{M}_{\mu_1\mu_2\mu_3\mu_4}(q_1, q_2 \rightarrow q_1, q_2) \quad (5)$$

$$= e^4 (-i\Pi_{\mu_1\mu_3\mu_4\mu_2}(-q_2; -q_1, q_1)).$$

* {green, hippel, meyerh, vladipas}@kph.uni-mainz.de

The forward scattering amplitude can be decomposed into eight Lorentz-invariant amplitudes [11]. They are functions of the virtualities q_1^2 and q_2^2 of the photons, as well as of the variable $\nu \equiv q_1 \cdot q_2$. Using the projector $R^{\mu\nu}$ onto the subspace orthogonal to q_1 and q_2 , we focus here on the amplitude [12]

$$\mathcal{M}_{\text{TT}}(q_1^2, q_2^2, \nu) = \frac{1}{4} R^{\mu_1\mu_3} R^{\mu_2\mu_4} \mathcal{M}_{\mu_1\mu_2\mu_3\mu_4}^{\text{forw}}(q_1, q_2). \quad (6)$$

Combining Eqs. (5) and (3), we can access the amplitude \mathcal{M}_{TT} from the Euclidean correlator,

$$\mathcal{M}_{\text{TT}}(-Q_1^2, -Q_2^2, -Q_1 \cdot Q_2) \quad (7)$$

$$= \frac{e^4}{4} R_{\mu_1\mu_3}^E R_{\mu_2\mu_4}^E \Pi_{\mu_1\mu_3\mu_4\mu_2}^E(-Q_2; -Q_1, Q_1),$$

$$R_{\mu\nu}^E \equiv \delta_{\mu\nu} - \frac{1}{(Q_1 \cdot Q_2)^2 - Q_1^2 Q_2^2} \cdot \quad (8)$$

$$\left[(Q_1 \cdot Q_2)(Q_{1\mu} Q_{2\nu} + Q_{1\nu} Q_{2\mu}) - Q_1^2 Q_{2\mu} Q_{2\nu} - Q_2^2 Q_{1\mu} Q_{1\nu} \right].$$

The largest value of $|\nu|$ that can be reached with Euclidean kinematics is limited by the virtualities of the photons [13], $|\nu| \leq (Q_1^2 Q_2^2)^{1/2} \leq \frac{1}{2}(Q_1^2 + Q_2^2) \equiv \nu_0$, while the nearest singularity is the s-channel π^0 pole located at $\nu_\pi = \frac{1}{2}(m_\pi^2 + Q_1^2 + Q_2^2)$. A technical issue arises when Q_1 and Q_2 are collinear: the projector $R_{\mu\nu}^E$ becomes ambiguous. To resolve the issue, we note that $R_{\mu\nu}^E = \bar{R}_{\mu\nu} - U_{1\mu} U_{1\nu}$, where $\bar{R}_{\mu\nu} \equiv \delta_{\mu\nu} - Q_{1\mu} Q_{1\nu} / Q_1^2$ and U_1 is the unit vector parallel to the projection of Q_2 onto the subspace orthogonal to Q_1 . The average of the applied projector over the directions of U_1 in that subspace yields

$$\langle \langle R_{\mu_1\mu_3}^E R_{\mu_2\mu_4}^E \rangle \rangle_{U_1} = \frac{2}{5} \bar{R}_{\mu_1\mu_3} \bar{R}_{\mu_2\mu_4} \quad (9)$$

$$+ \frac{1}{15} (\bar{R}_{\mu_1\mu_2} \bar{R}_{\mu_3\mu_4} + \bar{R}_{\mu_1\mu_4} \bar{R}_{\mu_3\mu_2}).$$

We use this averaged projector in Eq. (7) when Q_1 and Q_2 are collinear.

In [8], it was shown that the HLbL amplitude $\mathcal{M}_{\text{TT}}(\nu)$, for fixed spacelike photon virtualities, can be obtained from the following dispersive sum rule,

$$\mathcal{M}_{\text{TT}}(q_1^2, q_2^2, \nu) - \mathcal{M}_{\text{TT}}(q_1^2, q_2^2, 0) \quad (10)$$

$$= \frac{2\nu^2}{\pi} \int_{\nu_0}^{\infty} d\nu' \frac{\sqrt{\nu'^2 - q_1^2 q_2^2}}{\nu'(\nu'^2 - \nu^2 - i\epsilon)} (\sigma_0 + \sigma_2)(\nu'),$$

where σ_0 and σ_2 are the total cross sections $\gamma^*(q_1^2) \gamma^*(q_2^2) \rightarrow \text{hadrons}$ with total helicity 0 and 2 respectively. It can be shown [8] that \mathcal{M}_{TT} vanishes at $\nu = 0$ if either of the photons is real. It is interesting to test the sum rule for the π^0 pole contribution. Using the expression for $\Pi_{\mu\nu\rho\sigma}$ given in [14] and Eqs. (5, 6), one finds

$$\mathcal{M}_{\text{TT}}^{\pi^0}(-Q_1^2, -Q_2^2, \nu) = e^4 (\nu^2 - Q_1^2 Q_2^2) \quad (11)$$

$$\mathcal{F}(-Q_1^2, -Q_2^2)^2 \frac{Q_1^2 + Q_2^2 + m_\pi^2}{(Q_1^2 + Q_2^2 + m_\pi^2)^2 - 4\nu^2}$$

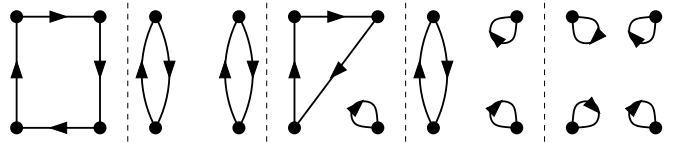


FIG. 1. Four-point function quark contraction topologies. The vertices represent vector currents and the lines are quark propagators. In this work, we compute only the leftmost, fully-connected class of diagrams.

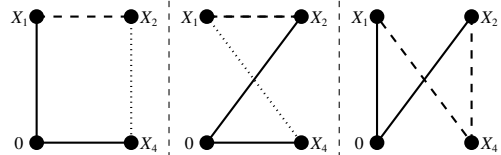


FIG. 2. Fully-connected four-point function quark contractions. Each panel represents two contractions with opposite directions of quark flow. The solid quark lines are computed using a point-source propagator, the dashed lines using sequential propagators, and the dotted lines using double-sequential propagators.

with $\mathcal{F}(q_1^2, q_2^2)$ the pion transition form factor as defined in [14]. For $q_2^2 = 0$, the same result is obtained from the sum rule, using the expression for the $\gamma\gamma^* \rightarrow \pi^0$ cross-section given in [8].

In summary, the amplitude \mathcal{M}_{TT} can be computed on the lattice via Eq. (7) and from e^+e^- collider data via Eq. (10). In the following, we present a comparison of the two approaches.

III. IMPLEMENTATION OF THE EUCLIDEAN FOUR-POINT FUNCTION IN LATTICE QCD

In numerical lattice QCD calculations of n -point functions, the quark path integral is evaluated analytically to yield a sum of contractions of quark propagators. For the four-point function of vector currents, these fall into five distinct topologies, illustrated in Fig. 1. In this work, we compute only the six contractions that are fully quark-connected.

We use a Wilson-type quark action, three lattice conserved currents J_μ^c and one site-local current J_μ^l (see for instance [15] for an explicit definition). Generically, we evaluate the fully-connected contribution to

$$\Pi_{\mu_1\mu_2\mu_3\mu_4}^{\text{lat}}(X_4; f_1, f_2) \equiv \sum_{X_1, X_2} f_1(X_1) f_2(X_2)$$

$$\langle J_{\mu_1}^c(X_1) J_{\mu_2}^c(X_2) J_{\mu_3}^l(0) J_{\mu_4}^c(X_4) + \text{contact terms} \rangle, \quad (12)$$

for some fixed functions $f_{1,2}$ and all values of $\{\mu_a\}$ and X_4 . The contact terms are present when two or three lattice conserved currents coincide, and serve to ensure that the conserved-current relations hold, e.g., $\Delta_{\mu_4}^{(X_4)} \Pi_{\mu_1\mu_2\mu_3\mu_4}^{\text{lat}} = 0$, where $\Delta_\mu^{(X)}$ is the backward lattice derivative.

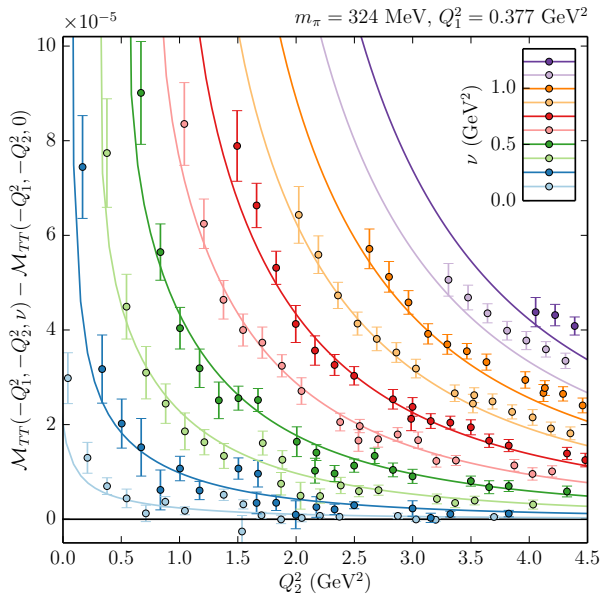


FIG. 3. The forward scattering amplitude \mathcal{M}_{TT} at a fixed virtuality $Q_1^2 = 0.377 \text{ GeV}^2$, as a function of the other photon virtuality Q_2^2 , for different values of ν . The curves represent the predictions based on Eq. (10), see the text for details.

The fully-connected contribution to Eq. (12) is evaluated using the method of sequential propagators. First, a point-source propagator is computed from X_3 . Then, it is combined with the function f_1 or f_2 to form the source for a new (sequential) propagator. These sequential propagators are then used to form sources for double-sequential propagators that depend on both f_1 and f_2 . Finally, the fully-connected contraction is formed using all three kinds of propagators; this is illustrated in Fig. 2. For generic complex f_1 and f_2 , this requires one point-source, 16 sequential and 32 double-sequential propagators, although these counts can be reduced in various special cases. We have verified that in our implementation the four-point function matches the lattice perturbation theory calculation if the gauge link variables are set to unity, and that the conserved-current conditions hold on each gauge configuration.

For evaluating the momentum-space correlator, we set the functions to be plane waves, $f_a(X) = e^{-iP_a \cdot X}$ and compute the Fourier modes with respect to X_4 . Thus, $\Pi_{\mu_1 \mu_2 \mu_3 \mu_4}^E(P_4; P_1, P_2)$ can be evaluated efficiently at fixed $P_{1,2}$ for all P_4 available on the lattice.

IV. RESULTS

We have used three lattice QCD ensembles with two degenerate flavors of non-perturbatively $\mathcal{O}(a)$ improved Wilson quarks and a plaquette gauge action. The ensembles are at a single lattice spacing $a = 0.063 \text{ fm}$ [16], correspond to pion masses $m_\pi = 451, 324$ and 277 MeV , and are respectively of spatial linear size 32, 48 and 48,

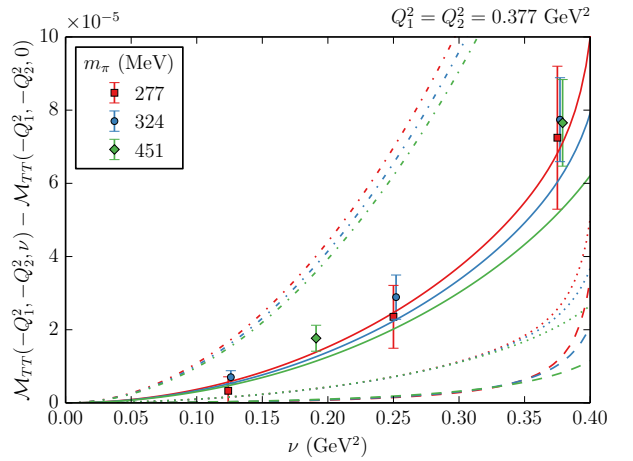


FIG. 4. The dependence of the amplitude \mathcal{M}_{TT} on ν , both photon virtualities being fixed at 0.377 GeV^2 , at three different pion masses. The dashed and dotted curves show the π^0 and $\pi^0 + \eta'$ contributions (there is no η meson in two-flavor QCD), the solid curve includes all single-meson and $\pi^+\pi^-$ contributions, and the dash-dotted curves additionally include the high-energy contribution for the case of real photons at the physical pion mass.

the time direction being twice as long; see [17] for more details. Only the up and down quark contributions to the electromagnetic current are included. The local vector current J_μ^l is renormalized non-perturbatively [18]. The results shown here were obtained using fairly low statistics, with a maximum of 300 samples.

Due to the finite volume of the lattice, the momenta take discrete values. The subtracted forward scattering amplitude, $\mathcal{M}_{\text{TT}}(-Q_1^2, -Q_2^2, \nu) - \mathcal{M}_{\text{TT}}(-Q_1^2, -Q_2^2, 0)$ (which is even in ν), is obtained by linearly interpolating the second term between the available Q_2^2 to match the first term. It is shown in Fig. 3 at fixed pion mass and fixed Q_1^2 , and also in Fig. 4 with both photon virtualities fixed. For the latter, linear interpolation in Q_2^2 was also used in the first term, except for the points at maximal ν . At fixed ν , the amplitude tends to decrease as the virtualities are increased, at fixed virtualities it tends to increase with $|\nu|$, and at fixed kinematics we do not find a significant dependence on the pion mass.

We compare the lattice data with results from the sum rule, Eq. (10), using a phenomenological model for the transverse $\gamma^*\gamma^* \rightarrow$ hadrons cross section, $\sigma_0 + \sigma_2$, based on Ref. [19]. We include pseudoscalar, scalar, axial-vector, and tensor mesons, as well as the non-resonant $\pi^+\pi^-$ contribution (in scalar treelevel QED with pion electromagnetic form factors). The $\gamma^*\gamma^* \rightarrow$ meson form factors have not been measured experimentally; they are assumed to factorize as $F(q_1^2, q_2^2) = F(q_1^2, 0)F(0, q_2^2)/F(0, 0)$. For the pseudoscalar and axial-vector mesons, $F(q^2, 0) = F(0, q^2)$ is described based on experimental data as in Ref. [8] and, lacking guidance from experiment, we assume a monopole form factor for the scalar and tensor resonances with a pole mass set by hand to $\Lambda = 1.6 \text{ GeV}$. The model is modified for unphys-

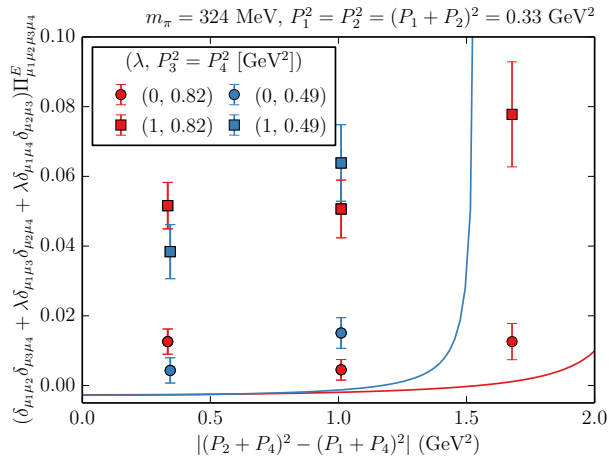


FIG. 5. Two Lorentz contractions of the vector four-point function at non-forward kinematics. For $\lambda = 1$ (squares), the pion pole contribution vanishes, while for $\lambda = 0$ (circles), it does not. The curves correspond to the π^0 pole contribution in the latter case.

ical quark masses by adjusting the masses and $\gamma\gamma$ decay widths, $\Gamma_{\gamma\gamma}$, of the mesons. The pion mass and decay constant [20] f_π are calculated on each lattice ensemble, and $\mathcal{F}(0,0)$ is set to the value $(-4\pi^2 f_\pi)^{-1}$ inspired by the chiral anomaly prediction (see e.g. [21]). For each of the remaining mesons, the mass is assumed to have the same shift as that of the ρ meson, relative to the physical point, and $\Gamma_{\gamma\gamma}$ is assumed to scale linearly with the meson's mass.

This model together with the dispersive sum rule produces the solid curves in Figs. 3 and 4, which agree well with the data. Varying Λ by ± 0.4 GeV shifts the curves by up to $\pm 50\%$, hence it is clear that the model has a considerable uncertainty; nevertheless the consistency with the data is remarkable. Fig. 4 also shows the individual contributions from π^0 and η' mesons and a high-energy contribution arising from a fit to the total $\gamma\gamma \rightarrow$ hadrons cross section [22] based on Regge theory. The latter is excluded from the main model curves due to the lack of a well-motivated extrapolation to the case of virtual photons and larger-than-physical pion masses. It is interesting to note that the two-pion production is typically the dominant contribution to the amplitude, rather than the π^0 and η' production.

Moving to off-forward kinematics, the situation is more complicated. In general, the four-point function of vector currents can be decomposed into 41 Lorentz-invariant functions [23] (see also [5]) that depend on six kinematic variables, of which three are fixed when P_1 and P_2 are fixed in our lattice calculation. To study the importance of the π^0 contribution, we consider two contractions: $\Pi_{\mu_1\mu_1\mu_3\mu_3}^E$, which has pion poles when $(P_1 + P_4)^2 = -m_\pi^2$ or $(P_2 + P_4)^2 = -m_\pi^2$, and a fully-symmetric contraction that has no π^0 -exchange contribution. These are shown

in Fig. 5, where we have also fixed $P_3^2 = P_4^2$ [where $P_3 = -(P_1 + P_2 + P_4)$] to be a typical hadronic scale below 1 GeV². We find that the fully-symmetric contraction yields larger data, again indicating that the π^0 does not provide the dominant contribution.

V. CONCLUSION

We have demonstrated that the fully connected contribution to the momentum-space four-point function of the electromagnetic current can be computed with moderate computational effort in lattice QCD if two of the three momenta are fixed. As an application, we computed one of the forward $\gamma^*\gamma^*$ scattering amplitudes in a broad kinematic range. Via a dispersive sum rule, it is related model-independently to $\gamma^*\gamma^* \rightarrow$ hadrons cross sections. Modelling the latter, we find the comparison of the lattice calculation with the phenomenological approach to be successful. The systematic uncertainties of the comparison are presently still large, mainly because our current calculations are performed at heavier quark masses than the physical ones, but this model dependence can be systematically reduced. Also, the not fully connected contraction topologies depicted in Fig. 1 could be important. We investigated the size of the pion pole contribution both in the forward and the off-forward amplitude. Both the lattice data and the model show that it is by no means dominant in a range of kinematic invariants of typical hadronic size.

The numerical methods presented can be applied to a direct lattice calculation of the HLbL contribution to $(g-2)_\mu$: we are currently working on a position-space approach where the photon propagators are integrated out semi-analytically in infinite volume. The dominant systematic effects are likely to be quite different from those in the method of Blum et al. [6], allowing for useful cross-checks. Since phenomenological calculations indicate that the π^0 is dominant in the HLbL contribution to $(g-2)_\mu$ [1], realistically light quark masses and large volumes will be required to treat this long-range contribution correctly. Lattice data on the HLbL amplitude itself can also help discriminate between phenomenological models used in the calculation of $(g-2)_\mu$.

ACKNOWLEDGMENTS

We thank A. Nyffeler, M. Vanderhaeghen and H. Wittig for helpful discussions. We are grateful for the access to the CLS lattice ensembles used here. The correlation functions were computed on the ‘Clover’ cluster at the Helmholtz-Institut Mainz. The programs were written using QDP++ [24] with the deflated SAP+GCR solver from openQCD [25].

-
- [1] T. Blum, A. Denig, I. Logashenko, E. de Rafael, B. Lee Roberts, *et al.*, (2013), arXiv:1311.2198 [hep-ph].
- [2] G. Venanzoni (Muon g-2), (2014), arXiv:1411.2555 [physics.ins-det].
- [3] V. Pauk and M. Vanderhaeghen, Phys.Rev. **D90**, 113012 (2014), arXiv:1409.0819 [hep-ph].
- [4] G. Colangelo, M. Hoferichter, M. Procura, and P. Stoffer, JHEP **1409**, 091 (2014), arXiv:1402.7081 [hep-ph].
- [5] G. Colangelo, M. Hoferichter, M. Procura, and P. Stoffer, (2015), arXiv:1506.01386 [hep-ph].
- [6] T. Blum, S. Chowdhury, M. Hayakawa, and T. Izubuchi, Phys.Rev.Lett. **114**, 012001 (2015), arXiv:1407.2923 [hep-lat].
- [7] V. Pascalutsa and M. Vanderhaeghen, Phys. Rev. Lett. **105**, 201603 (2010), arXiv:1008.1088 [hep-ph].
- [8] V. Pascalutsa, V. Pauk, and M. Vanderhaeghen, Phys.Rev. **D85**, 116001 (2012), arXiv:1204.0740 [hep-ph].
- [9] We use the notation and conventions of [26] unless otherwise stated. The metric is mostly minus. The fine-structure constant reads $\alpha \equiv e^2/(4\pi) \simeq 1/137$. The optical theorem for the scattering of scalar particles reads $\text{Im} \mathcal{M}(p_1, p_2 \rightarrow p_1, p_2) = 2E_{\text{cm}} p_{\text{cm}} \sigma_{\text{tot}}(p_1, p_2 \rightarrow \text{anything})$, with E_{cm} the total center-of-mass energy and p_{cm} the norm of the three-momentum of one of the particles in the center-of-mass frame.
- [10] We use capital letters to denote ‘Euclidean’ vectors, i.e. the metric in the scalar product of two such vectors is understood to be Euclidean.
- [11] V. M. Budnev, V. L. Chernyak, and I. F. Ginzburg, Nucl.Phys. **B34**, 470 (1971).
- [12] In the notation of [8], $\mathcal{M}_{\text{TT}} = \frac{1}{2}(M_{++,+} + M_{+,-,+})$ in terms of the helicity amplitudes. By virtue of the optical theorem, the imaginary part of \mathcal{M}_{TT} is proportional to the total unpolarized $\gamma^* \gamma^* \rightarrow \text{hadrons}$ cross-section. For the explicit expression of $R^{\mu\nu}$, see [11].
- [13] One might be able to extend the reach to $|\nu| = \nu_\pi$ with methods in the spirit of [27].
- [14] M. Knecht and A. Nyffeler, Phys.Rev. **D65**, 073034 (2002), arXiv:hep-ph/0111058 [hep-ph].
- [15] A. Francis, B. Jaeger, H. B. Meyer, and H. Wittig, Phys.Rev. **D88**, 054502 (2013), arXiv:1306.2532 [hep-lat].
- [16] S. Capitani, M. Della Morte, G. von Hippel, B. Knippschild, and H. Wittig, PoS **LATTICE2011**, 145 (2011), arXiv:1110.6365 [hep-lat].
- [17] P. Fritzscht, F. Knechtli, B. Leder, M. Marinkovic, S. Schaefer, *et al.*, Nucl.Phys. **B865**, 397 (2012), arXiv:1205.5380 [hep-lat].
- [18] M. Della Morte, R. Hoffmann, F. Knechtli, R. Sommer, and U. Wolff, JHEP **0507**, 007 (2005), arXiv:hep-lat/0505026 [hep-lat].
- [19] L.-Y. Dai and M. R. Pennington, Phys. Rev. D **90**, 036004 (2014).
- [20] G. P. Engel, L. Giusti, S. Lottini, and R. Sommer, Phys.Rev.Lett. **114**, 112001 (2015), arXiv:1406.4987 [hep-ph].
- [21] A. Bernstein and B. R. Holstein, Rev.Mod.Phys. **85**, 49 (2013), arXiv:1112.4809 [hep-ph].
- [22] K. A. Olive *et al.* (Particle Data Group), Chin.Phys. **C38**, 090001 (2014).
- [23] G. Eichmann, C. S. Fischer, and W. Heupel, (2015), arXiv:1505.06336 [hep-ph].
- [24] R. G. Edwards and B. Joó (SciDAC, LHPC, UKQCD), Nucl.Phys.Proc.Suppl. **140**, 832 (2005), arXiv:hep-lat/0409003 [hep-lat].
- [25] M. Lüscher, S. Schaefer, *et al.*, “openQCD,” <http://luscher.web.cern.ch/luscher/openQCD/>.
- [26] M. E. Peskin and D. V. Schroeder, *An Introduction to quantum field theory* (Addison-Wesley, Reading, USA, 1995).
- [27] X. Ji and C. Jung, Phys.Rev.Lett. **86**, 208 (2001), arXiv:hep-lat/0101014 [hep-lat].